X-ray topography study of LiB_3O_5 crystals grown from molybdate flux

2003 J. Phys.: Condens. Matter 15 6801

(http://iopscience.iop.org/0953-8984/15/40/016)

INSTITUTE OF PHYSICS PUBLISHING JOURNAL OF PHYSICS: CONDENSED MATTER

J. Phys.: Condens. Matter **15** (2003) 6801–6808 PII: S0953-8984(03)63778-1

X-ray topography study of LiB_3O_5 crystals grown from molybdate flux

A P Vasilenko[1], A V Kolesnikov[1], E M Trukhanov[1], N A Pylneva[2], A M Yurkin[2] and V V Atuchin[3]

[1] Department of Molecular Beam Epitaxy, Institute of Semiconductor Physics of SB RAS, Novosibirsk, 630090, Russia
[2] Laboratory of Crystal Growth, Institute of Mineralogy and Petrography of SB RAS, Novosibirsk, 630090, Russia
[3] Laboratory of Optical Materials and Structures, Institute of Semiconductor Physics of SB RAS, Novosibirsk, 630090, Russia

Received 20 May 2003
Published 26 September 2003
Online at stacks.iop.org/JPhysCM/15/6801

Abstract

The real defect structure of LiB_3O_5 crystal grown by a top seeded solution growth method has been observed using x-ray projection and reflective topography. Space mapping of such defects as growth sector boundaries, striation and dislocations have been produced by the topography analysis. The density of the dislocations is as low as <30 cm^{-2}. It has been shown that the dominant part of the dislocations detected is generated in the under-seed zone of the crystal.

1. Introduction

The combination of the wide range of transmission, large acceptance angle, moderate nonlinear optical coefficients and relative surface chemical stability allows extensive application of lithium triborate, LiB_3O_5 (LBO), in high-power nonlinear optical devices [1–4]. The LBO crystal is characterized by point space group $Pna2_1$ and the lattice parameters $a = 8.446(2)$ Å, $b = 7.380(2)$ Å and $c = 5.147(2)$ Å. The high laser damage threshold of LBO, up to $\sim$20 GW cm^{-2} for the bulk, opens up the possibility of using high-power pumping for efficient harmonic generation in visible and UV spectral ranges [5]. To decrease the scattering and divergence of the laser beams, very stringent requirements for the optical quality of LBO element should be fulfilled. First of all, the concentration of macroscopic defects in the crystal should be as low as possible. It is well known that $LiBO_3$ melts incongruently and the LBO crystal can be grown only by the flux method. Typically the excessive B_2O_3 in the melt is used as a solvent but, unfortunately, high viscosity is a characteristic of the flux [6–8]. This effect strongly limits the temperature range applicable for LBO crystal growth and stimulates the formation of foreign phase inclusions that degrade the crystal quality [9–12].

Recently, a polythermal section $Li_2O{\cdot}3B_2O_3$–MoO_3 was observed and the possibility of LBO growing from the MoO_3-based fluxes has been demonstrated [13]. Subsequently, the Li_2O–B_2O_3–MoO_3 ternary system was studied carefully to reveal the compositions feasible for LBO crystal growth by top seeded solution growth (TSSG) [14, 15]. The principal advantage of the molybdate-based solvents is the much lower viscosity of the melt in the temperature range suitable for LBO growth, compared with that of B_2O_3 flux. Under optimal growth conditions, large LBO crystals free of cracks, bubbles and inclusions have been grown. The typical size of optical quality crystals lies in the decimetre range and the weight is ∼500 g. The real defect structure of the crystals has been tested previously in [16] by x-ray powder diffraction and reflective topography methods. In parallel, the benefit of the application of MoO_3-based fluxes in the TSSG of borate crystals has been demonstrated for $M_xY_{1-x}Al_3(BO_3)_4$ (M = Yb, Dy), which is promising for the self-frequency-doubling (SFD) effect, and CuB_2O_4. In all these cases also, crystals of good quality have been produced [17–20]. The aim of the present study is the comprehensive observation of the bulk imperfections in LBO crystal grown from molybdate flux. X-ray projection and reflective topography have been applied as complementary tools because of the high sensitivity of the methods to such defects as inclusions, composition inhomogeneities and dislocations.

2. Experimental details

The LBO crystal was grown along the [001] direction by the TSSG method. High purity Li_2CO_3, B_2O_3 and MoO_3 powders were used for charge preparation. The flux was molten and homogenized at 900–950 °C for 16 h and then cooled to a temperature 20 °C above the saturation temperature. After the seed contacted the liquid surface the crystal was grown without pulling or rotation, with a flux cooling rate 0.5–1 °C/day until the temperature decreased to 700 °C. After this the crystal was extracted from the flux and cooled to room temperature over two days. The LBO crystal was confined by flat crystallographic faces and did not contain any visible defects. The schematic geometry of the crystal and the position of the (100) specimen studied in topography experiments are shown in figure 1. The plate, with thickness $t = 2$ mm, was cut through the zone near the seed position to reveal the effects induced by the initial stages of the crystal growth. Both sides of the plate were polished up to optical grade to remove the layer damaged by cutting.

X-ray transmission topographs were recorded using (004) and (060) reflections and Mo Kα radiation ($\lambda = 0.709$ Å) applying the Lang technique. For the sample the value of μt is equal to 0.4, where μ is the linear extinction coefficient of LBO. The double crystal reflection topographs were recorded using a (600) reflection and Cu Kα_1 radiation ($\lambda = 1.541$ Å). In this case the silicon (004) asymmetric monochromator provides a divergence of the incident beam below 1 arcsec. The reflection vectors $\mathbf{g}_{004}$, $\mathbf{g}_{060}$ and $\mathbf{g}_{600}$ used in the experiments are mutually orthogonal which ensures optimal conditions for revealing defects and strain fields in the crystal. So, the maximum topography contrast is observed for the lattice distortions with the direction of dominant deformation **e** parallel to **g** and the minimum contrast if the vectors **e** and **g** are orthogonal.

3. Results and discussion

Figures 2–4 show the transmission topographs for the LBO plate, and figure 5 shows a set of the reflection ones. The most prominent defect detected in figures 2–4 is the system of wide dark strips, which create an image of the curved rhomb ABCD, supplemented by the strips AA_1,

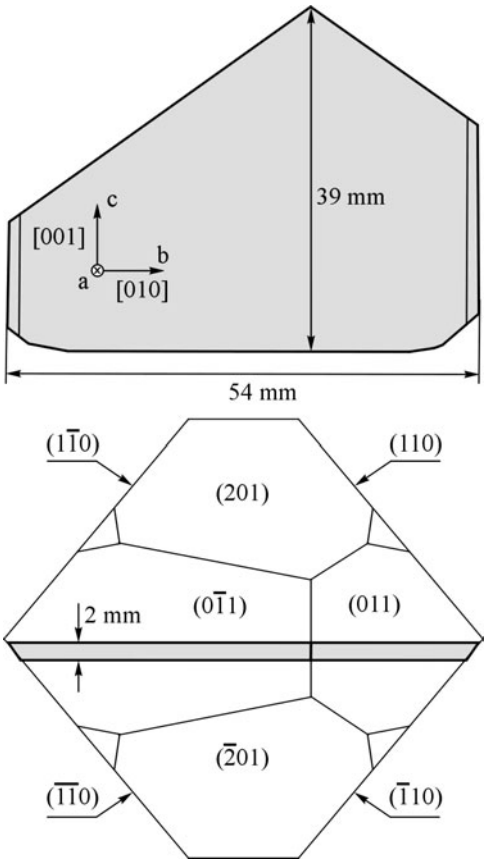

Figure 1. The shape and crystallographic orientation of the plate (a) and the morphology of LBO crystal (b). The plate position in the crystal body is shown in grey.

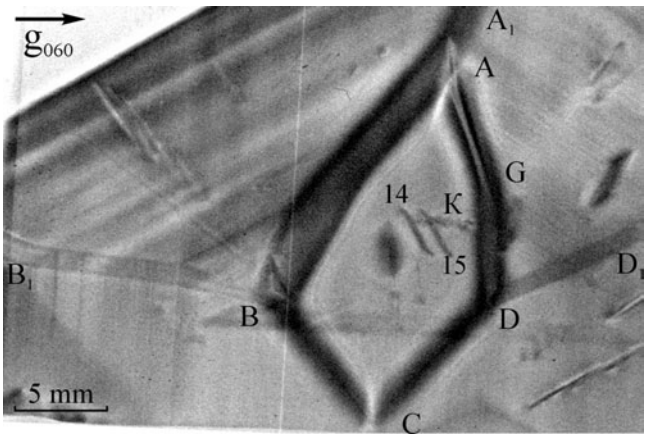

Figure 2. The projection topograph for $\mathbf{g}_{060}$.

BB_1, DD_1 with weak contrast. It is reasonable to say that during the crystal growth the seed was positioned 1–2 mm away from the point C in the approximate direction leading through

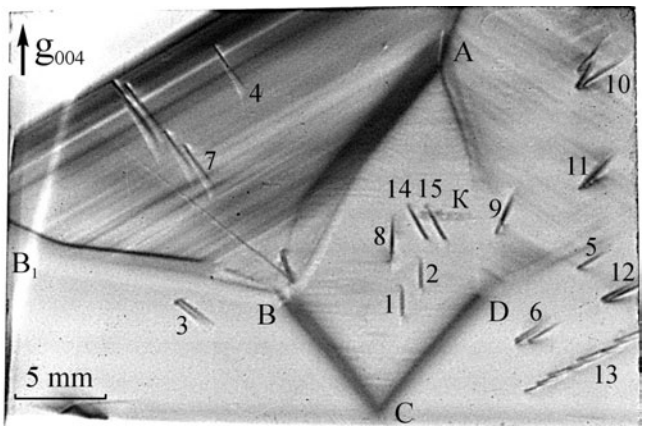

Figure 3. The projection topograph for $\mathbf{g}_{004}$.

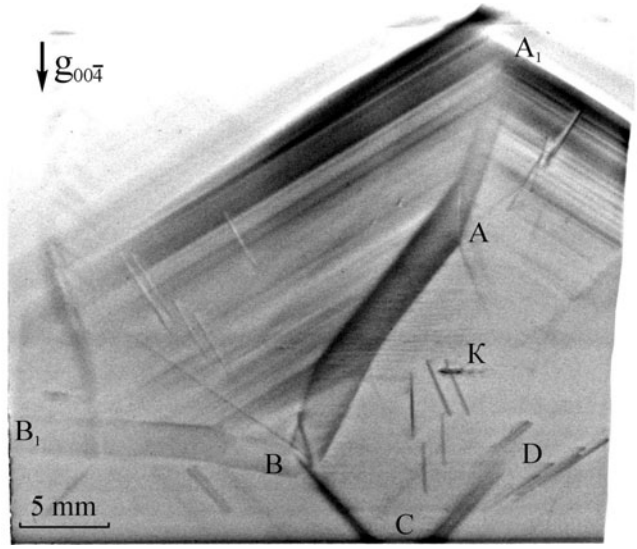

Figure 4. The projection topograph for $\mathbf{g}_{00\bar{4}}$.

the points A and C. Now, if you imagine the process of the crystal growth from the seed, then it is evident that the strips decorate the surfaces formed by the trajectories of the crystal edges moving during the process of the crystal growth. Taking into account figure 1(b), one can conclude that, for instance, the strip AB is formed by the edge, which is the intersection of the crystal faces $(\bar{2}01)$ and (011). This matching, as well as the results concerning the other moving edges, are summarized in table 1. It may be reasonably supposed that these dark strips are the growth sector boundaries. Typically the boundaries are characterized by an enhanced ability to capture foreign admixtures from the melt or increased concentration of lattice defects. Either of the mechanisms or both in combination may be the source of the contrast change in the topographs. As seen in figure 2, the two parts AG and GD form the strip AD. In figure 3, recorded using $\mathbf{g}_{004}$, the extinction of the strip GD is shown. Furthermore, near complete quenching of the line AD is evident in the topograph recorded for $\mathbf{g}_{00\bar{4}}$ (figure 4).

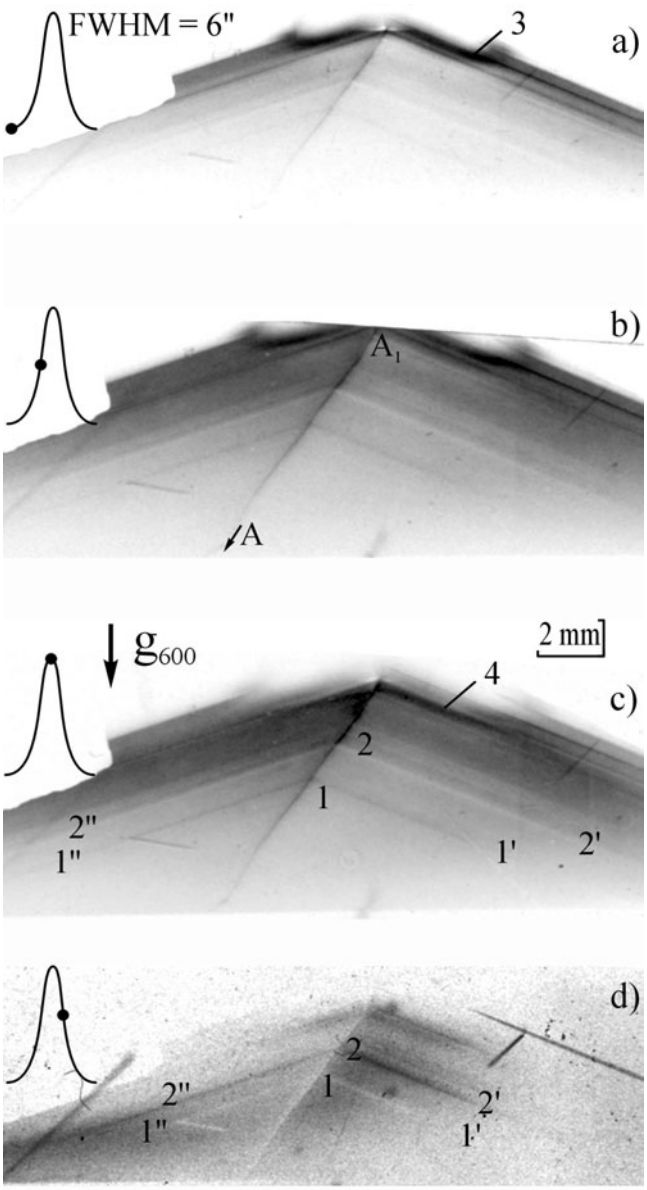

Figure 5. The reflective topographs for (600) reflection.

The quenching of the AD line contrast for $\mathbf{g}_{00\bar{4}}$, when the relation $\mathbf{eg} = 0$ is fulfilled, excludes the presence of such defects as foreign crystal phase precipitates in the ABCD rhomb contour. For the strip AD the dominant **e** occurs approximately in the plane (001).

The dark contrast of the above-mentioned wide strips in figures 2–4 is given by LBO crystal material but with gently modified cell parameters. Comparing the topographs with results in the literature, it may be supposed that a defect of the same type has been detected in the (001) plate in [12] for the LBO crystal also grown along the [001] direction. In the central part of the plate (figure 5 in [12]), in the under-seed zone, the group of inclusions is evident. This aggregate has clearly defined boundaries and is characterized by a deep dark

Table 1. The relationship between the strip notation in figures 2–5 and the edges of LBO crystal.

Strip	Edge
AB	$(\bar{2}01)$–(011)
BC	$(\bar{2}01)$–$(\bar{1}10)$
CD	$(\bar{2}01)$–$(\bar{1}\bar{1}0)$
DA	$(\bar{2}01)$–$(0\bar{1}1)$
AA_1	$(0\bar{1}1)$–(011)
BB_1	(011)–$(\bar{1}10)$
DD_1	$(0\bar{1}1)$–$(\bar{1}\bar{1}0)$

contrast. Around the inclusions the defects, like clouds with grey contrast, are visible with the contrast darkness decreasing as the point recedes from the centre. The clouds extend along the directions from the centre to the vertices of the sample. All the features correlate well with the characteristics of the moving edge defect structure in our sample.

Above the lines BB_1 and DD_1 numerous fine strips can be seen. The strips lie parallel to the crystal faces (011) and $(0\bar{1}1)$ with a change of direction on the line of the growth sector boundary AA_1 (see figure 4). As it appears, this defect system relates to the formation of segregation layers during the development of (011) and $(0\bar{1}1)$ crystal faces. Three particular fields in the plate are free of striation, namely, the interior of the rhomb ABCD and the areas below the lines BB_1 and DD_1. Evidently, the contrast becomes more pronounced and the strips become longer near the external crystal surfaces. It should be noted that the most developed part of the segregation strip structure can also be detected by optical methods.

More detailed observation of the strip structure was produced with the help of the reflectance topography method. A series of topographs is presented in figure 5. For comparison, on the left hand side of figure 5, the angle position of the crystal set in the (600) rocking curve is marked as it was during the topograph recording. To estimate the penetration of the x-ray wave into the crystal in this reflection geometry the extinction length was calculated. This is given by the relation $L_{\rm ext} = \lambda \sin\theta/2\pi|{\rm X_h}|C)$, where λ is the x-ray wavelength, θ is the Bragg angle, $\rm X_h$ is the polarization and C is the polarization factor [21]. The values of $L_{\rm ext}$ were estimated as 144 μm and 58 μm for π and σ polarization, respectively. These values are rather less than the LBO plate thickness (2 mm) and in figure 5 only the portions of the segregation strips and growth sector boundaries which are near the exit plate surface are visible.

The full width at half maximum (FWHM) of the rocking curve is 6 arcsec. Taking into account the fact that the value is measured with a very wide x-ray beam, 10×6 mm^2 in area, good structure uniformity of the sample is evident. The topographs 5(a)–(d) show the change of the contrast of the particular segregation strips 1–1′, 2–2′, 1–1″ and 2–2″ from dark to bright with the variation of the crystal angle position. In parallel the same contrast variations have been detected for the line AA_1, the growth sector boundary discussed above. One may conclude that for the strips 1′–1–1″ and for the growth AA_1 boundary the displacement vectors are closely related. Their sign is the opposite of that for the strips 2′–2–2″.

In free growth of LBO crystal the faces (011) and $(0\bar{1}1)$ are characterized by the lowest growth rate. So, the following mechanism of strip formation may be supposed. The absence of melt agitation results in local changes in melt composition or structure at the crystallization front in the directions [011] and $[0\bar{1}1]$; for instance, the continuous accumulation of some foreign admixtures may be supposed. Then, the fluctuations in the growth conditions induce variations in doping level or stoichiometry of the crystal with slight changes in cell parameters. In the topographs, the fluctuations manifest themselves as striation.

The next type of defect revealed in the LBO crystal is the grown-in dislocation. Defects are indicated by numbers in figures 2 and3. The structure K visible in figures 2–4 is a surface defect, appearing on the plate by manipulation. Taking the criteria of dislocation invisibility, the Burger's vector can be determined to define the dislocation character. So, dislocations 1 and 2 are of pure screw type with Burger's vector [001]. Dislocations 3–6 are characterized by the same Burger's vector but are of mixed type. In figure 2 images of dislocations 1–6 are extinguished synchronously. The edge components are the highest in magnitude and opposite in sign for dislocations 3 and 6. The lines, along which the dislocations 1–13 are running, cross in the vicinity of the seed, which was positioned near the point C. The only exception is the dislocation pair 14 and 15. So, as it seems that most of the dislocations were generated in the region near the seed during the initial stages of growth process. For comparison, it should be noted that earlier mainly more complicated dislocation systems with several directions have been observed in LBO [9, 10, 22]. It was also pointed out that many dislocations started from inclusions trapped from the flux. This mechanism of dislocation generation was also detected by topography in $M_xY_{1-x}Al_3(BO_3)_4$ (M = Yb, Dy) and BiB_3O_6 borate crystals [17, 19, 23]. In the LBO plate observed in our experiment the inclusions have not been detected and the estimated dislocation density is very low, not above $\sim$30 cm^{-2}. Moreover, large areas of the plate are dislocation free. Thus, the using of molybdate flux in LBO growth is promising for yielding dislocation-free crystals.

4. Conclusions

The defect structure of LBO crystal grown from molybdate flux and without melt agitation has been studied by means of x-ray topography methods. Three types of the defects were found: sector boundaries, growth striation and dislocations. The geometry of the defects is specified throughout the crystal body permitting us to define the parts with the best structure quality. So, it seems that using molybdate fluxes in the TSSG method is one way around the problem of high viscosity of B_2O_3-based fluxes that yields an enhancement of the real defect structure and optical homogeneity of borate crystals for high-power optics.

References

[1] Chen C, Wu Y and Li R 1990 The development of new NLO crystals in the borate series *J. Cryst. Growth* **99** 790–8

[2] Nikogosyan D N 1994 Lithium triborate (LBO): a review of its properties and applications *Appl. Phys.* A **58** 181–90

[3] Atuchin V V, Kesler V G, Lisova I A, Pokrovsky L D, Pylneva N A and Yurkin A M 2001 Stabilization of LiB_3O_5 crystal surfaces *Proc. SPIE* **4513** 107–13

[4] Jiang J and Hasama T 2002 High repetition-rate femtosecond optical parametric oscillator based on LiB_3O_5 *Opt. Commun.* **211** 295–302

[5] Furukawa Y, Markgraf S A, Sato M, Yoshida H, Sasaki T, Fujita H, Yamanaka T and Nakai S 1994 Investigation of the bulk laser damage of lithium triborate, LiB_3O_5, single crystals *Appl. Phys. Lett.* **65** 1480–2

[6] Zhao S, Huang C and Zhang H 1990 Crystal growth and properties of lithium triborate *J. Cryst. Growth* **99** 805–10

[7] Shumov D P, Nikolov V S and Nenov A T 1994 Growth of LiB_3O_5 single crystals in the Li_2O–B_2O_3 system *J. Cryst. Growth* **144** 218–22

[8] Zhong W and Tang D 1996 Growth units and morphology of lithium triborate (LBO) crystals *J. Cryst. Growth* **166** 91–8

[9] Zhao Q L, Huang Y S, Tang D Y, Jiang A D, Zhong W Z and Hua S K 1995 Study of growth defects and structure in nonlinear-optical crystals of lithium boric oxide *J. Appl. Crystallogr.* **28** 294–301

[10] Hu X B, Jiang S S, Huang X R, Zeng W, Liu W J, Chen C T, Zhao Q L, Jiang J H, Wang Z G, Tian Y L and Han Y 1996 The formation mechanisms of dislocations and negative crystals in LiB_3O_5 single crystals *J. Cryst. Growth* **163** 266–71

[11] Nihtianova D D, Shumov D P, Macicek J J and Nenov A T 1996 Inclusions in LiB_3O_5 crystals, obtained by the top-seeded solution growth method in the Li_2O–B_2O_3 system. Part II *J. Cryst. Growth* **169** 527–33

[12] Kim H G, Kang J K, Lee S H and Chung S J 1998 Growth of lithium triborate crystals by the TSSG technique *J. Cryst. Growth* **187** 455–62

[13] Parfeniuk C, Samarasekera I V, Weinberg F, Edel J, Fjeldsted K and Lent B 1996 Growth of lithium triborate crystals. II. Experimental results *J. Cryst. Growth* **158** 523–33

[14] Pylneva N A, Kononova N G, Yurkin A M, Bazarova G G and Danilov D I 1999 Growth and non-linear optical properties of lithium triborate crystals *J. Cryst. Growth* **198/199** 546–50

[15] Kosyakov V I, Pylneva N A, Bazarova Z G and Yurkin A M 2001 Topology of liquidus surface in B_2O_3–$Li_2O{\cdot}B_2O_3$–$Li_2O{\cdot}MoO_3$–MoO_3 system: implications to the growth of lithium triborate single crystals *Mater. Res. Bull.* **36** 573–84

[16] Pylneva N, Kosyakov V, Yurkin A, Bazarova G, Atuchin V, Kolesnikov A, Trukhanov E and Ziling C 2001 Real structure of LiB_3O_5 (LBO) crystals grown in Li_2O–B_2O_3–MoO_3 system *Cryst. Res. Technol.* **36** 1377–84

[17] Wang J, Hu X, Liu H, Li J, Jiang S, Zhao S, Teng B, Tian Y and Jiang J 2001 Growth and defects in $Yb_xY_{1-x}Al_3(BO_3)_4$ *J. Cryst. Growth* **229** 256–60

[18] Zhao S, Wang J, Sun D, Hu X, Li J, Liu Y and Wei J 2001 Morphology and growth mechanism of the $\{11\bar{2}0\}$ face of $Yb{:}YAl_3(BO_3)_4$ crystal *Surf. Rev. Lett.* **8** 685–8

[19] Martínez Vázquez R, Caballero M A, Gozález-Manas M, Kokanyan E P, Ruiz C M and Diéguez E 2002 Morphologic characterization of $Dy_xY_{1-x}Al_3(BO_3)_4$ single crystals grown from the flux and vapour phase *J. Cryst. Growth* **237–239** 668–71

[20] Alexandrov K S, Sorokin B P, Glushkov D A, Bezmaternykh L N, Burkov S I and Belushchenko S V 2003 Electromechanical properties and anisotropy of acoustic wave propagation in CuB_2O_4 copper metaborate *Phys. Solid State* **45** 41–5

[21] Tapfer L and Ploog K 1986 Improved assessment of structural properties of $Al_xGa_{1-x}As/GaAs$ heterostructures and superlattices by double-crystal x-ray diffraction *Phys. Rev.* B **33** 5565–74

[22] Zhao Q and Huang Y 1993 The dislocation fringes in crystals of lithium boric oxide *J. Mater. Sci. Lett.* **12** 932–4

[23] Teng B, Wang J, Cheng X, Wang Z, Jiang H, Dong S, Liu Y and Shao Z 2002 Growth defects in BiB_3O_6 crystals observed with white-beam synchrotron topography *J. Cryst. Growth* **235** 407–10